Surface Science 602 (2008) 3316–3322

Contents lists available at ScienceDirect

Surface Science

journal homepage: www.elsevier.com/locate/susc

Band-bending inhomogeneity of Au adsorbed Si(111)-$\sqrt{3} \times \sqrt{3}$-Ag surface evaluated with Si 2*p* core-level spectra

Canhua Liu [a,*], Iwao Matsuda [a,1], Toru Hirahara [a], Shuji Hasegawa [a], Jun Okabayashi [b], Satoshi Toyoda [b], Masaharu Oshima [b]

[a] Department of Physics, School of Science, University of Tokyo, 7-3-1 Hongo, Bunkyo-ku, Tokyo 113-0033, Japan
[b] Department of Chemistry, School of Engineering, University of Tokyo, 7-3-1 Hongo, Bunkyo-ku, Tokyo 113-0033, Japan

ARTICLE INFO

Article history:
Received 5 August 2008
Accepted for publication 2 September 2008
Available online 16 September 2008

Keywords:
Core-level spectrum photoemission
Si 2*p*
Superstructure
Band-bending
Charge transfer

ABSTRACT

Si 2*p* core-level spectra (CLS) of Au adsorbed Si(111)-$\sqrt{3} \times \sqrt{3}$-Ag surface at various Au coverages were measured using photoemission spectroscopy. At very low Au coverage where identical Au nanoclusters randomly distribute on the surface, the Si 2*p* CLS are reasonably decomposed, which implies the dispersed electrostatic potentials induced by the Au nanoclusters are strongly screened so that the inhomogeneity of the underlying band-bending is negligible. However, at a higher Au coverage where a part of Au nanoclusters aggregate into the Si(111)-$\sqrt{21} \times \sqrt{21}$-(Ag + Au) superstructure ($\sqrt{21}$-Au), the Si 2*p* CLS cannot be fully decomposed but be reproduced by combination of the CLS obtained from a pure Au nanocluster phase and a $\sqrt{21}$-Au phase. This indicates a strong band-bending inhomogeneity due to the partially aggregation of Au nanoclusters on the surface.

1. Introduction

Band-bending (BB) inhomogeneity is an important issue in the study of Schottky barrier formation, since it induces inhomogeneity in Schottky barrier height that strongly affect the electron transport properties at metal–semiconductor (MS) interfaces [1]. The BB inhomogeneity may also severely affect a lineshape of photoemission core-level spectrum (CLS) taken from a semiconductor surface where metal atoms sparsely adsorb thereon and act as potential centers altering the BB locally. This has been experimentally demonstrated by Cimino et al. on metal-covered GaAs(110) surface [2] and by De Renzi et al. on K adsorbed H:Si(111)(1 × 1) surface [3]. In both cases, the BB inhomogeneity modifies the lineshape of CLS significantly and makes them impossible to be fully decomposed. On a metal terminated semiconductor surface with metallic surface-state bands, by contrast, the sparsely distributed potential (adatoms) may be well screened by the surface-state electrons so that BB inhomogeneity would be negligible. In spite of its reasonableness, however, this conjecture has not been testified in experiment yet.

A monolayer-Ag-terminated Si(111), the Si(111)-$\sqrt{3} \times \sqrt{3}$-Ag surface ($\sqrt{3}$-Ag hereafter), adsorbed by an extremely low density of Au atoms, is a particularly suitable system for studying this issue. The $\sqrt{3}$-Ag surface is a good substrate due to its high intrinsic homogeneity and low defect density, which is reflected in the sharpness of its Si 2*p* CLS. Moreover, being a two-dimensional (2D) electron gas system, the $\sqrt{3}$-Ag surface has a metallic surface-state band with parabolic dispersion crossing the Fermi level [4–6]. After extensive studies including photoelectron spectroscopy (PES) [4–8], first-principles calculation [9–11], scanning tunneling microscopy (STM) [12,13], X-ray diffraction [14,15] and other experimental techniques [16,17], the $\sqrt{3}$-Ag surface has been well known and become popular as a substrate for adsorption of various metal atoms [5,18–21] and molecules [22–25]. Au atoms were chosen as adsorbates because they form identical 2D nanoclusters, which distribute randomly on the $\sqrt{3}$-Ag surface at the extremely low Au coverage (named as Au *nanocluster phase*), as Fig. 1a shows [26]. As the Au coverage increases, a part of 2D nanoclusters aggregate into the Si(111)-$\sqrt{21} \times \sqrt{21}$-(Ag + Au) superstructure ($\sqrt{21}$-Au hereafter), resulting in a *mixed phase* (Fig. 1b). The $\sqrt{21}$-Au superstructure covers the whole surface uniformly at a saturate Au coverage, 0.14 monolayer (ML), inducing a $\sqrt{21}$-Au *phase* (Fig. 1c).

In this study, we measured the Si 2*p* CLS of Au adsorbed $\sqrt{3}$-Ag surface to evaluate the BB inhomogeneity in different Au adatom phases. In the Au nanocluster phase where only Au nanoclusters sparsely distribute on the surface, the Si 2*p* CLS are reasonably resolved. This implies a negligible BB inhomogeneity resulting from a

* Corresponding author. Present address: International Center for Young Scientists, National Institute for Materials Science, 1-1 Namiki, Tsukuba, Ibaraki 305-0044, Japan.
E-mail address: liu.canhua@nims.go.jp (C. Liu).
[1] Present address: Institute for Solid State Physics, University of Tokyo, 5-1-5 Kashiwa-no-ha, Kashiwa, Chiba 277-8581, Japan.

0039-6028/$ - see front matter © 2008 Elsevier B.V. All rights reserved.
doi:10.1016/j.susc.2008.09.011

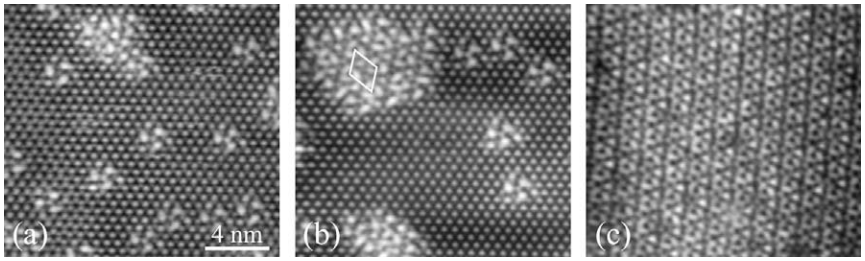

Fig. 1. Topographic STM images of Au adsorbed $\sqrt{3}$-Ag surface at various Au coverages, θ_{Au}, showing different Au adatom phases: (a) Au nanocluster phase at θ_{Au} = 0.02 ML, V_{tip} = 0.5 V; (b) mixed phase at θ_{Au} = 0.04 ML, V_{tip} = −0.3 V and (c) $\sqrt{21}$-Au phase at θ_{Au} = 0.14 ML, V_{tip} = 1.5 V. The same tunneling current of I = 0.75 nÅwas set. More STM images and detailed discussion on the self-assembly of Au nanoclusters are available in reference [26].

strong screening of the electrostatic potentials induced by the Au nanoclusters. The influenced area of each Au-induced potential is limited to the first Si layer and estimated to be less than 1– 2 nm from the center of each Au nanocluster. At intermediate Au coverages for the mixed phase, the Si 2*p* CLS can not be reasonably resolved. By combination of CLS taken from a pure Au nanocluster phase and a $\sqrt{21}$-Au phase, we successfully reproduce the CLS of the mixed phase. This indicates that the underlying BB in the mixed phase is inhomogeneous due to the difference in BB in the two pure phases.

2. Experiment

The PES experiment was performed in a UHV chamber (base pressure: better than 5×10^{-11} Torr) installed on the beam line BL-1C at the Photon Factory in KEK, Tsukuba, Japan. The chamber is equipped with a low-energy electron diffraction (LEED) system and an analyzer of Scienta SES-100 with an energy resolution of ~20 meV. The sample surface was prepared in a same manner as we did in previous report [26]. A B-doped *p*-type Si(1 1 1) wafer with resistivity of 1–10 Ω cm at RT was used. After outgassing at ~400 °C throughout a night, the wafer was electrically flashed at 1250 °C to obtain a clean Si(1 1 1)-7 × 7 surface. The $\sqrt{3}$-Ag surface was produced at a substrate temperature of 450 °C by depositing 1 ML Ag atoms. Two minutes' post-annealing at the deposition temperature was proceeded to improve the quality of the $\sqrt{3}$-Ag surface. After deposition of Au atoms at RT, sample surfaces were transported to another stage kept at 70 K for CL PES measurement.

The adsorption rate of Au atoms is roughly calibrated with LEED by making a sequence of Au/Si(1 1 1) phases at optimal coverages [27,28]: 5×2 (0.44 ML), α-$\sqrt{3} \times \sqrt{3}$(2/3ML) and β-$\sqrt{3} \times \sqrt{3}$ phases (1 ML). More precise Au coverages were determined from the Au 4*f* CLS taken at normal emission with photon energy of 135 eV (see Fig. 2a), by comparing the intensity with that of an optimized surface, Si(1 1 1)-5 × 2-Au.

3. Results and discussion

According to our recent STM observations [26] (see also Fig. 1), each Au nanocluster consists of three Au adatoms that sit on equivalent sites at the $\sqrt{3}$-Ag surface, exhibiting three-fold symmetry. This means all Au adatoms have identical chemical environment so that photoelectrons emitted from CL states of Au atoms can be easily resolved. To verify it, we measured the Au 4*f* CLS at various Au coverages on the $\sqrt{3}$-Ag surface, as shown in Fig. 2a. Two spin–orbit splitting peaks are identified in each spectrum. All the Au 4*f* CLS can be reproduced well by Voigt line shape added to a linear background. A typical resolved result of the Au 4*f* CLS at 0.145 ML, where a clear $\sqrt{21} \times \sqrt{21}$ LEED pattern has been observed, is shown in Fig. 2b. There are two components being recognized: the grey component dominates the spectrum while the black one is negligibly small. It can be simply explained by assigning the grey component to the Au atoms adsorbed on well defined sites of the $\sqrt{3}$-Ag substrate, while the black one to Au defect atoms adsorbed, for example, on steps of the Si surface. Thus, one main component is enough for fitting the raw data of the Au 4*f* CLS, which is consistent with our STM observations mentioned before.

Fig. 3 is a summary of the Si 2*p* CLS taken from the Au/$\sqrt{3}$-Ag surfaces at various Au coverages. LEED patterns, which agree with the previous STM measurements, are also described in the figure. "No $\sqrt{21} \times \sqrt{21}$" at 0.016 ML and 0.021 ML in Fig. 3 means that no $\sqrt{21} \times \sqrt{21}$ LEED pattern was observed (only $\sqrt{3} \times \sqrt{3}$ pattern), corresponding to the Au nanocluster phase discovered in the STM observations (see Fig. 1a). At 0.060 ML and 0.037 ML, the LEED patterns showed a series of faint $\sqrt{21} \times \sqrt{21}$ spots due to small $\sqrt{21}$-Au domains in the mixed phase (see Fig. 1b). When the Au coverage reached 0.145 ML, the LEED pattern exhibited very sharp $\sqrt{21} \times \sqrt{21}$ spots, indicating that the surface was covered by large $\sqrt{21}$-Au domains. At 0.322 ML, however, the $\sqrt{21} \times \sqrt{21}$ LEED pattern became faint again since the excess Au atoms partially destroy the $\sqrt{21}$-Au.

The Si 2*p* CLS shift gradually toward higher binding energy as Au coverage increases, indicating that Au adatoms modify BB of the Si substrate gradually. This is because Au adatoms dope the $\sqrt{3}$-Ag surface with electrons, elevating the Fermi level and thus softening the BB. The correlation of BB with surface band structures was reported previously [29,30], so here we concentrate on the BB inhomogeneity, which correlates strongly to the topographic distribution of Au adatoms. Actually, the lineshapes of the Si 2*p* CLS have a strong "phase dependence" rather than a Au coverage dependence. Both in the Au nanocluster phase and $\sqrt{21}$-Au phase where only one type of phase domain exists, the CLS is insensitive to the Au coverage, *i.e.*, the CLS lineshape at 0.016 ML (0.145 ML) is similar to that at 0.021 ML (0.191 ML). In the mixed phase, however, the CLS changes a lot in shape from 0.037 ML to 0.060 ML. This can be naturally understood with the fact that Si 2*p* CL photoelectrons emitted from Au nanocluster phase domains and $\sqrt{21}$-Au domains contribute two different lineshapes of CLS. When the Au coverage within the mixed phase changes, the intensity ratio of the CLS from the two different Au phase domains varies accordingly, resulting in the change in the CLS lineshape.

We have tried to resolve all the CLS shown in Fig. 3. However, only those taken from the phases of bare $\sqrt{3}$-Ag, Au/$\sqrt{3}$-Ag nanocluster and $\sqrt{21}$-Au, but not from the mixed phase, can be reasonably decomposed, as Fig. 4 shows. The parameters used in the resolving procedure are summarized in Tables 1 and 2. In the following, we first discuss the resolvable Si 2*p* CLS in various pure phases, and then turn to the irresolvable ones in the mixed phase, to obtain the information of BB inhomogeneity in each Au adatom phase.

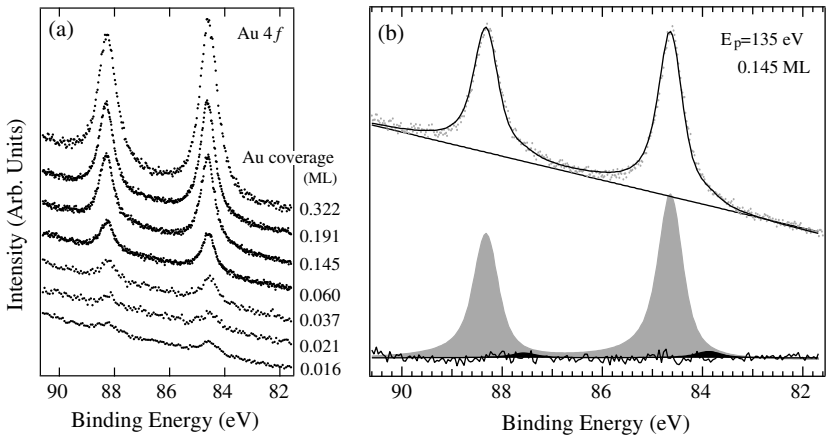

Fig. 2. Au 4*f* CLS of the Au/$\sqrt{3}$-Ag surfaces, recorded at normal emission with photon energy of 135 eV. (a) shows the raw data for various Au coverages; (b) shows the resolved result of the spectrum at 0.145 ML, where $\sqrt{21}$-Au domains cover the whole surface. Voigt line shapes are used in the fitting procedure with the following parameters: spin–orbit splitting is 3.68 eV, branching ratio 0.75; singularity 0.05, Gaussian width 0.30 eV, and Lorentzian width 0.40 eV.

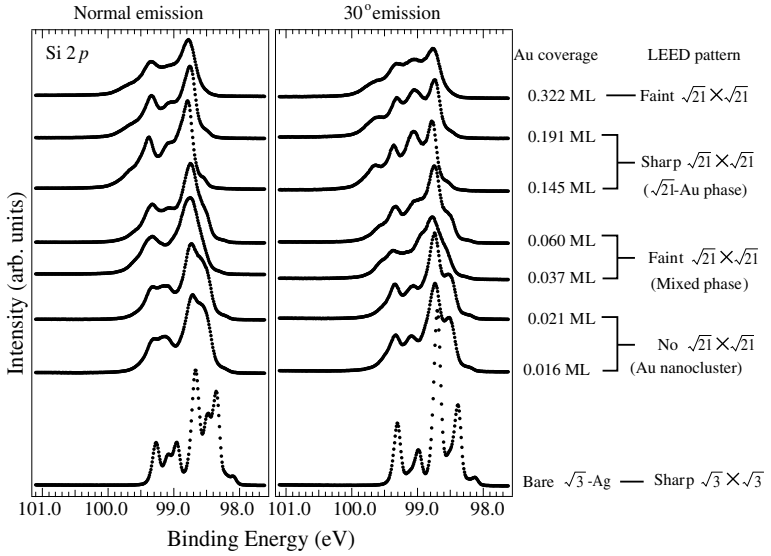

Fig. 3. Summary of the Si 2*p* CLS of the Au/$\sqrt{3}$-Ag surfaces at various Au coverages, recorded at normal (left panel) and 30° (right panel) emissions with photon energy of 135 eV. The LEED pattern of each sample surface is described in correspondence to its Au coverage.

3.1. Surface superstructures of $\sqrt{3}$-Ag and $\sqrt{21}$-Au

In both $\sqrt{3}$-Ag and $\sqrt{21}$-Au phases, the superstructures uniformly cover the whole surface and thus modify the substrate BB homogeneously. We succeeded in decomposing the Si 2*p* CLS (see Fig. 4a and b and e and f), which have been reported previously in the construction of the $\sqrt{21}$-Au atomic structure model [26]. Here, we briefly summarize the decomposition results for the purpose of a further discussion on the Si 2*p* CLS taken from the other two Au adatom phases.

The Si 2*p* CLS of the bare $\sqrt{3}$-Ag surface is decomposed into two surface (C_1 and C_2), one bulk (B) and one defect (D) components. The two surface components of C_1 and C_2 are assigned to the first and second layer Si atoms, respectively, as shown in Fig. 5a. The third layer Si atoms are in a bulk-like environment and may not give rise to any significant energy shift in the spectra.

Similar to those of the bare $\sqrt{3}$-Ag surface, the Si 2*p* CLS of the $\sqrt{21}$-Au phase are resolved with three surface (R_1, R_2 and R_3), one bulk (B) and one defect (D) components. Based on our newly proposed atomic structure model, in which Au atoms sit on the Ag triangle centers of the unaltered $\sqrt{3}$-Ag framework [26], we assigned that both R_1 and R_3 are from the first layer Si atoms while R_2 from the second layer, as shown in Fig. 5b. The first layer Si atoms are thus divided into two groups: one bonds with the Ag triangles adsorbed by Au adatoms (R_3 component), while the other with the bare ones (R_1 component). It is noted that a very recent first-principles calculation suggests that the Au adatoms immerse in the Ag layer and the Ag triangles be modified [31]. Because the calculation agrees that the Au adatoms are supported by a part of Ag triangles, it doesn't conflict with our conclusions from the Si 2*p* CLS experiments.

3.2. Au nanocluster phase

In the Au nanocluster phase (see Fig. 1a), the sparsely distributed Au nanoclusters are positively charged by doping the substrate with electrons, and thus expected to induce BB inhomogeneity. According to the previous studies on metal-covered GaAs(1 1 0) surface and K adsorbed H:Si(1 1 1)(1 × 1) surface, [2,3], the Si 2*p* CLS should be difficult for decomposition, since it requires a large number of components with various energy shifts due to the BB inhomogeneity. However, we succeeded in resolving the CLS taken at both 0.016 ML and 0.021 ML with only several components. This implies the Au-induced electrostatic potential

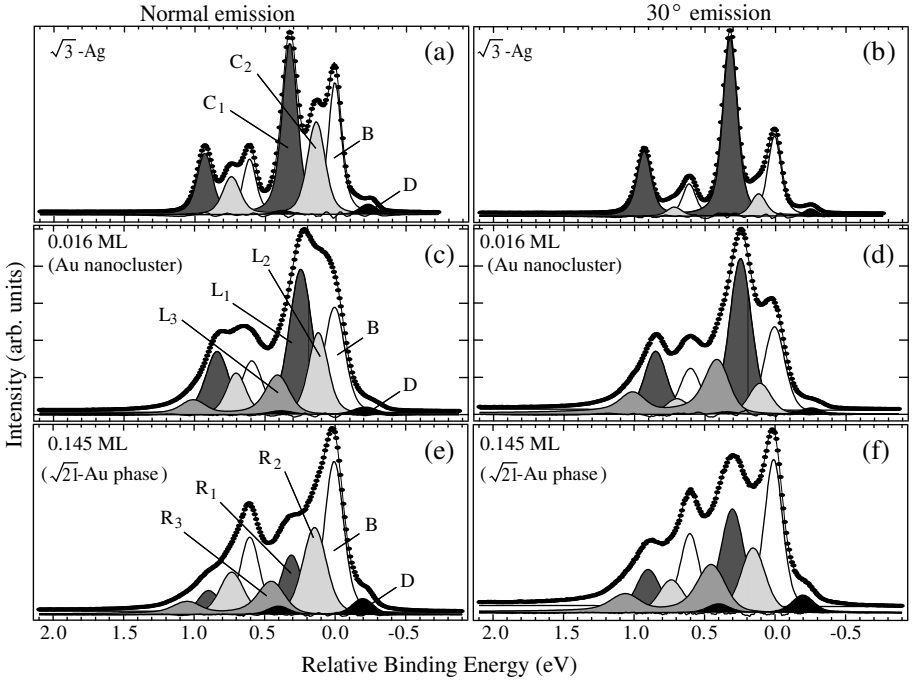

Fig. 4. Resolved results of the Si 2*p* CLS taken from the $\sqrt{3}$-Ag surface, (a) and (b), the Au nanocluster phase at θ_{Au} = 0.016 ML, (c) and (d), and the $\sqrt{21}$-Au phase at θ_{Au} = 0.145 ML, (e) and (f). Note that in order to compare the energy shift of each component in the resolved results, relative binding energy is used in the horizontal axis. The $2p_{1/2}$ binding energy of the bulk components (0 eV in the figure) in the three phases, $\sqrt{3}$-Ag, Au nanocluster and $\sqrt{21}$-Au, is 98.36 eV, 98.48 eV and 98.76 eV, respectively.

Table 1
Summary of the parameters used in resolving the Si 2*p* CLS shown in Fig. 4

Parameters	$\sqrt{3}$-Ag	0.016 ML	0.145 ML
SO splitting (eV)	0.605(3)	0.594(6)	0.595(5)
Branching ratio	0.38(2)	0.44(5)	0.41(3)
Singularity	0	0.04	0.04
Lorenzian (meV)	80	80	80
Gaussian (meV)	B: 65	B: 110	B: 110
	$C_{1,2}$:95(10)	$L_{1,2}$:150(10)	$R_{1,2}$:150(10)
		L_3:180	R_3: 180

Other two parameters are shown in Table 2 in detail for discussion.

Table 2
Relative binding energy and relative intensity optimized in resolving the Si 2*p* CLS shown in Fig. 4

Surface	Component	Relative binding energy (eV)		Relative intensity		
		0°	30°	0°		30°
$\sqrt{3}$-Ag	B	0	0	0.30	↘	0.27
	C_1	0.32	0.31	0.42	↗	0.62
	C_2	0.13	0.11	0.26	↘	0.08
	D	−0.24	−0.27	0.02		0.03
Nanocluster	B	0	0	0.27	↘	0.25
(0.016 ML)	L_1	0.24	0.24	0.39	↗	0.43
	L_2	0.12	0.10	0.20	↘	0.09
	L_3	0.40	0.40	0.12	↗	0.22
	D	−0.22	−0.26	0.02		0.01
$\sqrt{21}$-Au	B	0	0	0.41	↘	0.37
(0.145 ML)	R_1	0.31	0.30	0.16	↗	0.25
	R_2	0.14	0.15	0.27	↘	0.18
	R_3	0.44	0.44	0.13	↗	0.16
	D	−0.20	−0.20	0.03		0.04

The arrows in the table indicate increase (↗) or decrease (↘) in the relative intensity of the respective components when the emission angle changes from 0° to 30°.

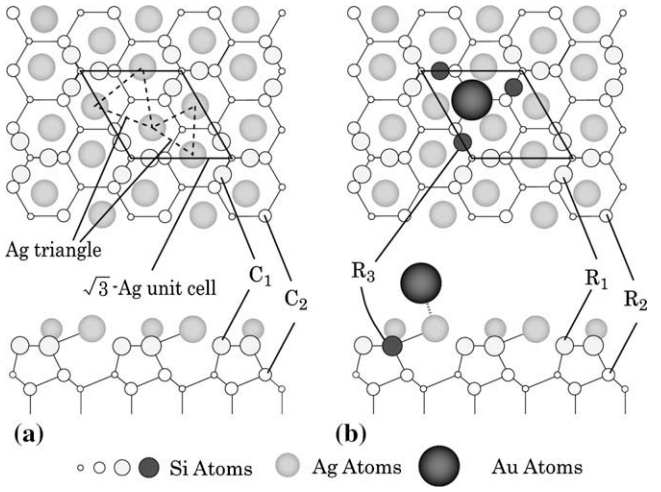

Fig. 5. Atomic structure models of the $\sqrt{3}$-Ag surface used for interpreting the resolved results of the Si 2*p* CLS shown in Fig. 4. (a) is for the bare $\sqrt{3}$-Ag surface, and (b) is for the Au adsorbed case.

should be strongly screened, resulting in a homogeneous BB beneath the $\sqrt{3}$-Ag surface.

Figs. 4c and 4d show only the resolved results of 0.016 ML because those of 0.021 ML are the same. Both spectra taken at normal and 30° emissions are decomposed into three surface (L_1, L_2 and L_3), one bulk (B) and one defect (D) components. The binding energies of all the components are independent on the emission angles (Table 2), implying the reasonableness of the decomposition. Irrespective of an extremely small number of Au adatoms thereon, the CLS lineshape changes dramatically in the transition from the bare $\sqrt{3}$-Ag to the Au nanocluster phase, while the resolved components have some similarities. For example, the relative intensities of the bulk components in both phases are similar. The component L_2 has also very similar relative binding energies

and relative intensities with C_2 for both emission angles (see Table 2), which implies that L_2 also originates from the second layer Si atoms as C_2 does. Moreover, since the sum of their relative intensities is comparable to that of C_1, the components L_1 and L_3 are believed to originate from the first layer Si atoms as C_1 does. These assignments are convinced by the fact that all the components arising from a same layer Si atoms change in relative intensity in the same manner when emission angle is changed. As indicated by the arrows in Table 2, the relative intensities of all the components from the first layer Si atoms (C_1, $L_{1,3}$ and $R_{1,3}$) increase as emission angle changes from 0° to 30°, while those from the second layer (C_2, L_2 and R_2) decrease simultaneously.

It is noted that the binding energy of L_1 (0.24 eV) is smaller while that of L_3 (0.40 eV) is larger than that of C_1 (0.32 eV). This is obviously caused by the sparsely distributed Au nanoclusters on the surface (see Fig. 1a). The Au adatoms transfer unlocalized electrons to the substrate, so that the first-layer Si atoms far from the Au adatoms may have a more negatively charged environment than those of the bare surface, contributing to L_1 with a lower binding energy. The first-layer Si atoms near the Au adatoms, on the contrary, may have a more positively charged environment due to the attractive potential induced by the Au cations, thus contribute to L_3 with a higher binding energy.

The influenced area of the Au-induced potential can be roughly estimated from the relative intensity of the related components. Giving I_{L1} and I_{L3} to be the relative intensities of L_1 and L_3, respectively, the ratio of the influenced area to the whole surface is estimated to be

$$\frac{I_{L3}}{I_{L3}+I_{L1}} = \frac{0.12}{0.12+0.39} = 24\%. \quad (1)$$

Here we used the resolved results of the normal-emission CLS listed in Table 2 as an example. Since the Au coverage is 0.016 ML, the concentration of isolated Au nanoclusters is $4.2 \times 10^{16}\ m^{-2}$, noticing three Au atoms per Au nanocluster. The influenced area of the attractive potential is thus estimated to be $24\%/(4.2 \times 10^{16}) = 5.7 \times 10^{-18}\ m^2$. This value can be approximated to a circular area with a radius of 1.3 nm. The same estimating procedure was also carried on the 30°-emission CLS and those at other Au coverages. As a conclusion, the radius of the influenced area of the potential induced by one Au nanocluster is estimated to be 1–2 nm. This value is comparable to the size of the Au nanocluster, indicating that the potential influence on the CLS from the first-layer Si atoms is limited to very small areas around the Au nanoclusters. Actually, this is a reasonable result considering that the Au-induced electrostatic potentials may be strongly screened by the surrounding 2D free-like electrons. Ono et al. [32] have directly observed such a screen effect with scanning tunneling spectroscopy on the $\sqrt{3}$-Ag surface, showing that the electrostatic potential exhibits a strong distance dependence only in a circular area with a radius of ~2 nm, which is consistent with our current estimations.

It is worth emphasizing that the component L_2 from the second Si layer has an almost identical relative binding energy with C_2 of the bare $\sqrt{3}$-Ag surface. Moreover, it does not split into two components as C_1 does. These facts indicate that the influence of the Au-induced electrostatic potentials is limited within only the first Si layer. Si atoms in the second or deeper layers have little changes in chemical environment caused by the sparsely distributed electrostatic potentials. In other words, the BB inhomogeneity possibly introduced by the Au adatoms is negligible. At even lower Au coverage (less than 0.016 ML shown here), the lineshapes of Si 2*p* CLS may be slightly different due to a reduction in intensity of L_3 components, and they may shift toward lower binding energy on the whole due to smaller electron doping from Au adatoms to the $\sqrt{3}$-Ag surface. However, the above discussion on the negligibleness of BB inhomogeneity is still applicable because the screen effect does not depend on the Au coverage in the nanocluster phase. This contrasts well with the cases of meta-covered GaAs(1 1 0) and K adsorbed H:Si(1 1 1)(1 × 1) surfaces, where there is no free-like electrons to screen the adatom-induced potentials so that the BB inhomogeneity is significantly exhibited in those CLS lineshape [2,3].

3.3. Mixed phase

As mentioned before, the Si 2*p* CLS taken from the mixed phase can not be decomposed in a reasonable way. In addition, they change obviously in lineshape when Au coverage varies, as the dotted curves shown in Fig. 6. These facts are obviously due to the coexistence of Au nanocluster domains and $\sqrt{21}$-Au domains at the surface (see Fig. 1b), so the CLS of the mixed phase have to be reproduced in a different way.

The binding energy of the bulk component shifts due to the Au adsorption, which can be directly observed in Fig. 3 from the peak shifts of the Si 2*p* CLS as the Au coverage varies. It is noted that the "bulk" component here corresponds to the Si atoms in the space-charge layer very close to the surface, rather than those in the deep bulk crystal. Therefore, we can obtain the modification of BB induced by Au adatoms from the binding energy shift of the bulk component in Si 2*p* CLS. After resolving the spectra shown in Fig. 4, the binding energy of the bulk Si $2p_{1/2}$ state was obtained to be 98.36 eV, 98.48 eV and 98.76 eV for $\sqrt{3}$- Ag, Au nanocluster and $\sqrt{21}$-Au phases, respectively. In a rigid-band model for the bulk electronic structure close to the surface, the valence band maximum (VBM) shifts in the same way as the Si 2*p* CL state does. Since the VBM at the $\sqrt{3}$-Ag surface has been reported to be 0.l6 eV below the Fermi level [29], we can thus obtain the VBM at the surfaces in Au nanocluster and $\sqrt{21}$-Au phases to be 0.28 eV and 0.56 eV, respectively. These results indicate that the BB is quite different between the two phases, since the VBM in deep bulk is fixed and independent of surface structure.

In the mixed phase, therefore, the BB is inhomogeneous due to the coexistence of Au nanocluster and $\sqrt{21}$-Au domains. The inhomogeneity may be large enough for significant modification of the Si 2*p* CLS since the difference in BB between the two domains is 0.28 eV, which is comparable to the relative binding energies of the surface components (see Table 2). Consequently, CL states of Si atoms beneath different domains may have different binding energies even if they are in a same layer, so that the Si 2*p* CLS contain too much components with various energy shifts to be fully resolved.

In a simplified case, the local BB may be homogeneous within a single domain as long as the domain size is not too small, and its value in different domains of the same type should be identical. In other words, only two types of BB exist in the surface if domain boundaries are ignored. In this case, the Si 2*p* CL photoelectrons emitted from the mixed phase can be classed into two groups depending on their binding energy: one is from Au nanocluster domains and the other from $\sqrt{21}$-Au domains. This means the measured Si 2*p* CLS of the mixed phase is the combination of those from the two pure phases.

We verified the above idea by combining the Si 2*p* CLS taken at 0.016 ML (Au nanocluster phase) and at 0.145 ML ($\sqrt{21}$-Au phase) to reproduce those of the mixed phase, as Fig. 6 shows. In the combination, the CLS of the two pure phases are shrunken due to the decrease in their corresponding domain areas at the mixed phase. Although the absolute value of the contribution from each component CLS to the combined CLS is meaningless due to the imperfect normalization of the CLS intensity, the trend of change in the contribution with respect to the Au coverage is very reasonable in the current combination; When the Au coverage is increased from 0.037 ML to 0.06 ML in Fig. 6, the contribution of the

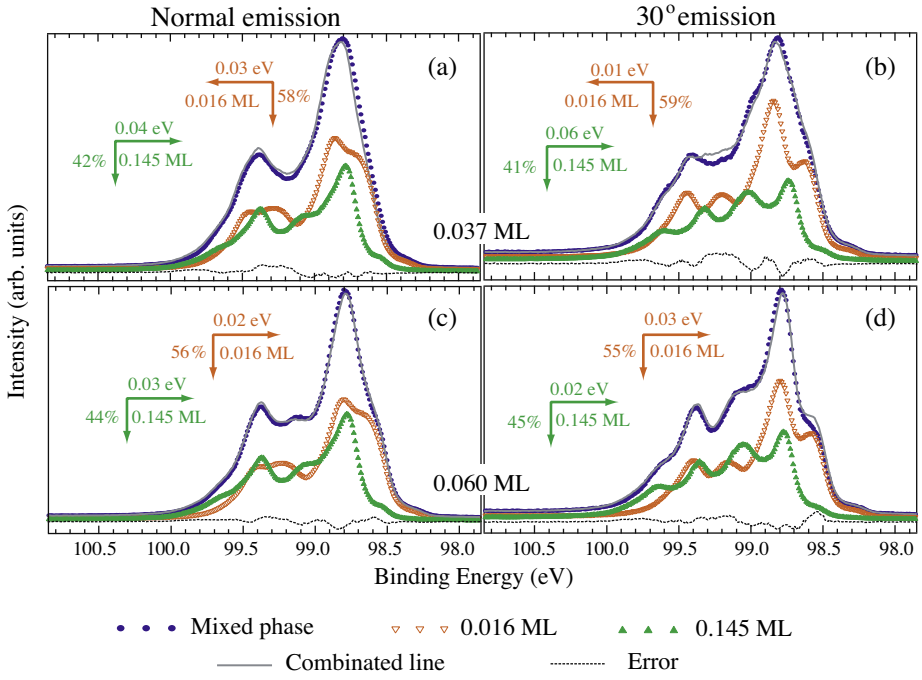

Fig. 6. Si 2*p* CLS of the Au/$\sqrt{3}$-Ag surfaces at the mixed phase at θ_{Au} = 0.037 ML, (a) and (b), and θ_{Au} = 0.060 ML, (c) and (d).

$\sqrt{21}$-Au CLS (0.145 ML) to the mixed-phase CLS is increased while that of the Au-nanocluster CLS (0.016 ML) is decreased both in normal and 30° emission data. The parallel arrows in Fig. 6 indicate the energy shifts of respective CLS in combination. They are all negligible considering the energy resolution of the experiment. This implies that the BB of a single domain at the mixed phase is identical to that of its corresponding pure phase.

The combination results are shown with grey curves in Fig. 6, which reproduces well the Si 2*p* CLS of the mixed phase, as expected. This result also confirms our assumption that the areas of domain boundaries containing intermediate BB due to continuity are small enough to be neglected.

4. Conclusions

The Si 2*p* CLS of the Au/$\sqrt{3}$-Ag surfaces have been measured at various Au coverages to evaluate the BB inhomogeneity of the Si substrate. At the Au nanocluster phase where Au nanoclusters sparsely distribute on the surface, the Si 2*p* CLS are reasonably decomposed in spite of the dispersed electrostatic potentials induced by the Au nanoclusters. The resolved results imply that the BB inhomogeneity in this phase is negligible since the electrostatic potentials are strongly screened by the 2D free-like electron gas at the $\sqrt{3}$-Ag surface. The influence of the Au induced potentials on the Si atoms is limited to the first Si layer and within areas of no more than 1–2 nm from the centers of the Au nanoclusters. At mixed phase where the Au nanocluster and the $\sqrt{21}$-Au domains coexist, the Si 2*p* CLS are well reproduced, in spite of strong BB inhomogeneity, by combination of those taken from the Au nanocluster and the $\sqrt{21}$-Au phases. It indicates that the BB in a single domain (the Au nanocluster or the $\sqrt{21}$-Au domain) at the mixed phase is identical to that of its corresponding pure phase.

Acknowledgements

K. Sakamoto and T. Okuda are sincerely appreciated for valuable advices in experiments and data analysis. This work has been supported by Grants-In-Aid from the Japanese Society for the Promotion of Science (JSPS) and A3 Foresight Program of JSPS-KOSEF-NSFC.

References

[1] R.T. Tung, Phys. Rev. B 45 (1992) 13509;
R.T. Tung, Appl. Phys. Lett. 58 (1991) 2821.
[2] R. Cimino, A. Giarante, K. Horn, M. Pedio, Europhys. Lett. 32 (1995) 601.
[3] V. De Renzi, R. Biagi, U. del Pennio, M. Pedio, A. Goldoni, R. Larciprete, Phys. Rev. B 62 (2000) R10657.
[4] L.S.O. Johansson, E. Landemark, C.J. Karlsson, R.I.G. Uhrber, Phys. Rev. Lett. 63 (1989) 2092.
[5] C. Liu, I. Matsuda, R. Hobara, S. Hasegawa, Phys. Rev. Lett. 96 (2006) 036803.
[6] T. Hirahara, I. Matsuda, M. Ueno, S. Hasegawa, Surf. Sci. 563 (2004) 191.
[7] I. Matsuda, H. Morikawa, C. Liu, S. Ohuchi, S. Hasegawa, T. Okuda, T. Kinoshita, C. Ottaviani, A. Cricenti, M. D'angelo, P. Soukiassian, G. Le Lay, Phys. Rev. B 68 (2003) 085407.
[8] R.I. Uhrberg, H.M. Zhang, T. Balasubramanian, E. Landemark, H.W. Yeom, Phys. Rev. B 65 (2002) 081305.
[9] S. Watanabe, M. Aono, M. Tsukada, Phys. Rev. B 44 (1991) 8330.
[10] Y.G. Ding, C.T. Chan, K.M. Ho, Phys. Rev. Lett. 67 (1991) 1454.
[11] H. Aizawa, M. Tsukada, N. Sato, S. Hasegawa, Surf. Sci. Lett. 429 (1999) L509.
[12] N. Sato, T. Nagao, S. Hasegawa, Surf. Sci. 442 (1999) 65.
[13] L. Chen, H.J. Xiang, B. Li, A. Zhao, X. Xiao, J. Yang, J.G. Hou, Q. Zhu, Phys. Rev. B 70 (2004) 245431.
[14] T. Takahashi, S. Nakatani, N. Okamoto, T. Ishikawa, S. Kikuta, Jpn. J. Appl. Phys. 27 (1988) L753;
T. Takahashi, S. Nakatani, N. Okamoto, T. Ishikawa, S. Kikuta, Surf. Sci. 242 (1991) 54.
[15] H. Tajiri, K. Sumitani, S. Nakatani, A. Nojima, T. Takahashi, K. Akimoto, H. Sugiyama, X. Zhang, H. Kawata, Phys. Rev. B 68 (2003) 035330.
[16] H. Nakahara, T. Suzuki, A. Ichimiya, Appl. Surf. Sci. 234 (2004) 292.
[17] Y. Fukaya, A. Kawasuso, A. Ichimiya, e.-J. Surf. Sci. Nanotechnol. 3 (2005) 228.
[18] S. Hasegawa, X. Tong, S. Takeda, N. Sato, T. Nagao, Prog. Surf. Sci. 60 (1999) 89.
[19] C. Liu, S. Yamazaki, R. Hobara, I. Matsuda, S. Hasegawa, Phys. Rev. B 71 (2005) 041310(R).
[20] H. Hibino, T. Ogino, Phys. Rev. B 54 (1996) 5763.
[21] I. Matsuda, T. Hirahara, M. Konishi, C. Liu, H. Morikawa, M. D'angelo, S. Hasegawa, T. Okuda, T. Kinoshita, Phys. Rev. B 71 (2005) 235315.
[22] J.A. Theobald, N.S. Oxtoby, M.A. Phillips, N.R. Champness, P.H. Beton, Nature 424 (2003) 1029. and references therein.
[23] M.A. Phillips, J.N. O'Shea, P.R. Birkett, J. Purton, H.W. Kroto, D.R.M. Walton, R. Taylor, P. Moriarty, Phys. Rev. B 72 (2005) 075426.
[24] L. Wang, K. Schulte, R.A.J. Woolley, M. Kanai, T.J.S. Dennis, J. Purton, S. Patel, S. Gorovikov, V.R. Dhanak, E.F. Smith, B.C.C. Cowie, P. Moriary, Surf. Sci. 564 (2004) 156.
[25] G. Hughes, D. Carty, O. McDonald, A.A. Cafolla, Surf. Sci. 580 (2005) 167.

[26] C. Liu, I. Matsuda, M. D'angelo, S. Hasegawa, J. Okabayashi, S. Toyoda, M. Oshima, Phys. Rev. B 74 (2006) 235420.
[27] R. Plass, L.D. Marks, Surf. Sci. 380 (1997) 497.
[28] T. Nagao, K. Tsuchie, S. Hasegawa, S. Ino, Phys. Rev. B 57 (1998) 10100.
[29] X. Tong, C.S. Jiang, S. Hasegawa, Phys. Rev. B 57 (1998) 9015.
[30] J.N. Crain, M.C. Gallagher, J.L. McChesney, M. Bissen, F.J. Himpsel, Phys. Rev. B 72 (2005) 045312.
[31] H. Jeong, H.W. Yeom, S. Jeong, Phys. Rev. B 76 (2007) 085423.
[32] M. Ono, Y. Nishigata, T. Nishio, T. Eguchi, Y. Hasegawa, Phys. Rev. Lett. 96 (2006) 016801.